10.2 AN ENERGY-DIAGNOSTICS INTERCOMPARISON OF COUPLED ICE-OCEAN ARCTIC MODELS

Petteri Uotila *, David M. Holland
New York University, New York, NY
Sirpa Häkkinen
NASA/Goddard Space Flight Center, Greenbelt, MD
Greg Holloway, Nadja Steiner
Institute of Ocean Sciences, Sidney, BC, Canada
Michael Steele, Jinlun Zhang
University of Washington, Seattle, WA
Andrey Proshutinsky
WHOI, Woods Hole, MA

1. INTRODUCTION

The Arctic Ocean Model Intercomparison Project (AOMIP) is an international collaborative effort that has been established to perform a detailed analysis of the performance of state-of-the-art coupled ice-ocean models of the Arctic Ocean (Proshutinsky et al. (2001); Steele et al. (2001a)). The AOMIP www-site is located at the URL: http://fish.cims.nyu.edu/project_aomip/overview.html .

One important diagnostic of model performance is the total energy content within a model domain and the manner in which that energy is distributed in its various forms, such as kinetic, potential, and internal (see for example Ivchenko et al. (1997)). Quantifying the sources and sinks of energy is also an important aspect of obtaining an overall energy budget for the model domain. Energy intercomparison provides high-level information of the model parameterizations of mixing processes, thermohaline circulation, currents, and river freshwater input. The energy transport between the Arctic and mid-latitudes is an especially crucial parameter (Peixoto et al. (1992)). Understanding the links between the polar regions and the global climate system strengthens our understanding of the Arctic Ocean energy balance.

This paper is based on a manuscript by Uotila et al. (2003), which is submitted to *Ocean Modelling* journal. Following the manuscript, some steps toward a comprehensive accounting and intercomparison of the energy budgets for the various AOMIP models are reported.

2. METHODS

We follow closely the formulation by Oort et al. (1994) (hereinafter O94) in our analysis. However, the aim of our study is quite different: while O94 estimated the large-scale global energetics, we focus on the differences of the Arctic Ocean models. O94 relied on the observed climatology, while we utilize model results, which, however, were initialized according to hydrographic climatologies. In addition the models represent the sea-ice covered Arctic region, which was excluded by O94.

The kinetic energy of the models is estimated from the monthly velocity fields. In addition to the annual average KE fields the areas of the highest variability are compared. An accurate eddy kinetic energy (EKE) analysis is not possible due to the low temporal accuracy and resolution of the model data.

The kinetic energy (KE) is defined as

$$KE = \frac{1}{2}\int_V \rho \mathbf{c}^2 dV, \tag{1}$$

where ρ is the density of ocean, $\mathbf{c}$ is the velocity vector of the water motion and V is the basin volume.

The balance of KE is

$$\frac{\partial KE}{\partial t} = G(KE) + C(APE,KE) + C(IE,KE) - D(KE), \tag{2}$$

where $G(KE)$ is the generation rate of KE due to the external forcing, such as atmospheric momentum and lateral boundary fluxes. $C(APE,KE)$ is the rate of conversion from potential energy to KE, and $C(IE,KE)$ denotes the conversion from internal energy into KE. Following O94, $C(IE,KE)$ is considered to be very small compared to the other terms, and is excluded from the analysis. $D(KE)$ represents dissipation of KE.

The total potential energy (PE) is defined as

$$PE = \int_V \rho g z dV, \tag{3}$$

where z is the vertical coordinate and g is the acceleration due to gravity. We calculate APE following the definition

$$APE = PE - \int_V \rho_r g z_r dV, \tag{4}$$

where the second term on the right represents a reference potential energy RPE that is subtracted from PE.

* *Corresponding author address:* Petteri Uotila, Courant Institute of Mathematical Sciences, New York Univ., 251 Mercer Street, New York, NY, 10012; e-mail: uotila@cims.nyu.edu

The reference level z_r is defined to correspond to the minimum potential energy state (Huang (1998); Winters et al. (1995)).

Oort et al. (1989) utilized a formula for APE following from a quasi-geostrophic approximation as

$$APE_O = -\frac{1}{2}\int_V g(\rho - \tilde{\rho})^2 (\frac{\partial \widetilde{\rho_\phi}}{\partial z})^{-1} dV. \quad (5)$$

Here $\widetilde{\ }$ represents the horizontal averaging operator and ρ_ϕ is the potential density respect to the surface. $\partial\rho_\phi/\partial z$ the vertical gradient of ρ_ϕ. Notice that the APE estimated following (5) is hereinafter referred as APE_O.

The monthly energy rate $\frac{\partial APE}{\partial t}$ is estimated as differences of monthly APE values. The balance of APE is

$$\frac{\partial APE}{\partial t} = G(APE) - C(APE, KE) - D(APE), \quad (6)$$

where $G(APE)$ is the generation rate of APE due to the external forcing, such as sensible and latent heat fluxes and lateral boundary fluxes. $D(APE)$ represents dissipation of APE and can be estimated following O94.

Conversion from available potential to kinetic energy $C(APE, KE)$ is

$$C(APE, KE) = -g\int_V (\rho - \tilde{\rho}) w dV, \quad (7)$$

where w is the vertical velocity component of the velocity field $\vec{v} = (u, v, w)$.

The internal heat energy (IE) is defined as

$$IE = \int_V c_o \rho T dV, \quad (8)$$

where c_o, is the specific heat at constant pressure for ocean waters and T is the water temperature.

3. DATA

For the analysis a region approximatively common to all the models was chosen (Figure 1). No interpolations to a common grid are done, because this would increase uncertainty of derived results and conclusions, and is not a straightforward task. Because models have their specific coordinate systems the comparison regions are not exactly same.

Four models (IOS, UW, GSFC, and NYU models) are compared in this particular study: IOS model originates in the Institute of Ocean Science, Sidney, Canada; UW model is from the University of Washington, Seattle, USA; GSFC model is from the NASA/Goddard Space Flight Center, Greenbelt, USA; and the NYU model is from the New York University, New York. The characteristics of the models and particular model runs studied in this paper are listed in Table 1. One may note that the vertical coordinate system varies between the models: IOS and UW models utilize a z-coordinate system, GSFC a σ-coordinate system and NYU a ρ-coordinate system.

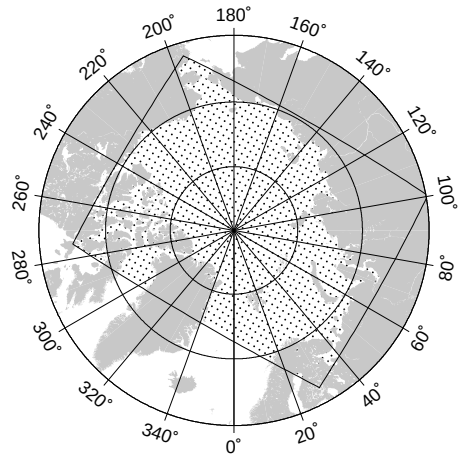

Figure 1: The common intercomparison area for all models is outlined by the rectangular box. That area is represented by a latitude-longitude grid with 1° spatial resolution and has rotated latitude-longitude coordinates with respect to true geographical latitude-longitude coordinates. It is referred as the AOMIP grid.

AOMIP models were forced in general with different data, and physical and numerical parameters varied as well. For example, the atmospheric forcing was constructed either from National Centers for Environmental Predictions (NCEP) reanalysis, or European Centre for Medium-Range Forecasts Re-Analysis 40 (ECMWF, ERA-40), or from observed data of International Arctic Buoy Programme/Polar Exchange at the Sea Surface (IABP/POLES). Additionally IOS, GSFC, and UW models take river discharge into consideration, which is parameterized in the NYU model as an artificial climate restoring term. The NYU, GSFC, and UW models cover a larger area than the IOS model.

The IE and APE_o fields derived from the Polar Science Center Hydrographic Climatology v2.1 (PHC 2.1, Steele et al. (2001b)) are utilized in the comparison. The PHC data is plotted in Figures 2 and 3 for comparison with the model results. Earlier versions of PHC was also used for initial conditions of IOS and NYU models (Table 1).

We estimate the magnitudes of the energy components and rates (in J m^{-2} and W m^{-2}, respectively) of the energy cycle by applying values for ocean depth H $= 10^3$ m, water density $\rho_w = 1025$ kg m^{-3}, horizontal velocity $u = 0.01$ m s^{-1}, vertical velocity $w = 10^{-6}$ m s^{-1}, temperature $T = 275$ K, specific heat capacity $c_o = 3950$ J kg^{-1} K^{-1}.

Table 1: Model descriptors.

Model	Reference	δx	vert. dims.	Atm. forcing data (year/climatology)	Initial conditions
GSFC	Häkkinen (1999)	$0.9^\circ \times 0.7^\circ$	σ-coord. 20 levels	ECMWF: 1998	Levitus (1994)
IOS	Holloway and Sou (2002)	$1/2^\circ \times 1/2^\circ$	z-coord. 29 levels	NCEP reanalysis: climatological mean	PHC December
NYU	Holland (2001)	$1^\circ \times 1^\circ$	ρ-coord. 11 layers	ECMWF reanalysis climatological mean	PHC 1.0
UW	Zhang et al. (2000)	40 km	z-coord. 21 levels	IABP/POLES: 1998	Levitus (1994)

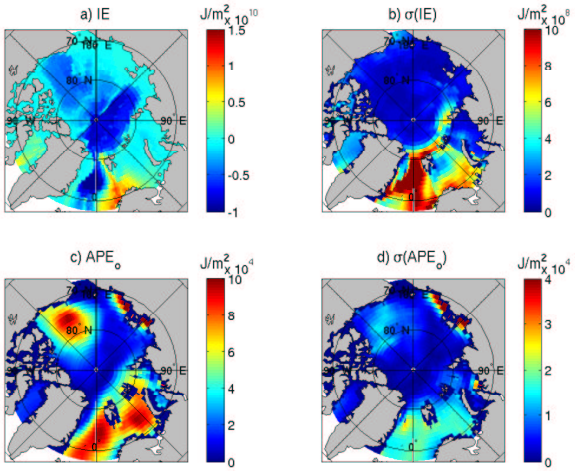

Figure 2: Annual fields of (a) average internal heat energy, (b) deviation of internal heat energy, (c) average available potential energy APE_o, and deviation of available potential energy APE_o for PHC 2.1 updated from Steele et al. (2001b). Note that the coordinates refer to the geographical grid. Also note that the temperature data applied in the computation of (a) is relative to the 0°C.

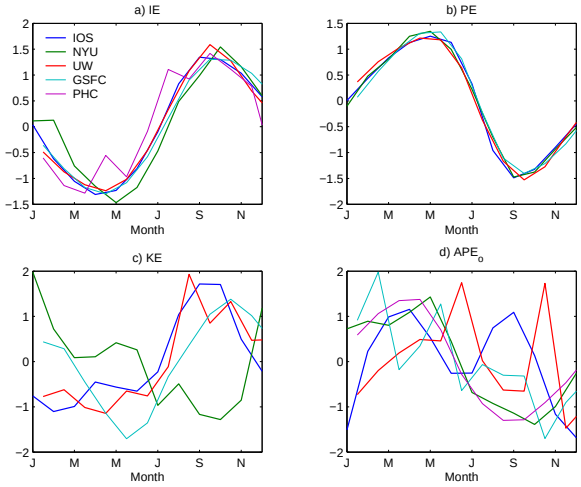

Figure 3: Seasonal normalized time series of (a) internal heat energy, (b) potential energy, (c) kinetic energy, and (d) available potential energy APE_O.

4. RESULTS

4.1 *Internal heat energy*

The modeled internal heat of the Arctic basin is the energy component that has the best mutual correspondence between the models. The average values are relatively close to each other, 1.3 - 1.4$\times 10^{12}$ J m^{-2}, while the deviation is about one magnitude smaller. These are in correspondence with the estimated magnitude of $IE = \rho_w c_o TH \simeq 10^{12}$ J m^{-2}. The seasonal cycles of IE provided by the models are quite coherent as presented in Figure 3a, with IE minimums after the winter in April-May, and increasing values through the summer until the fall. The NYU model cycle deviates the most from the others. In Figure 3 the cycles are normalized by subtracting the mean value and dividing by the standard deviation, because the model runs represent varying forcing conditions and periods and thus the absolute energy values are not as directly comparable as the normalized time series.

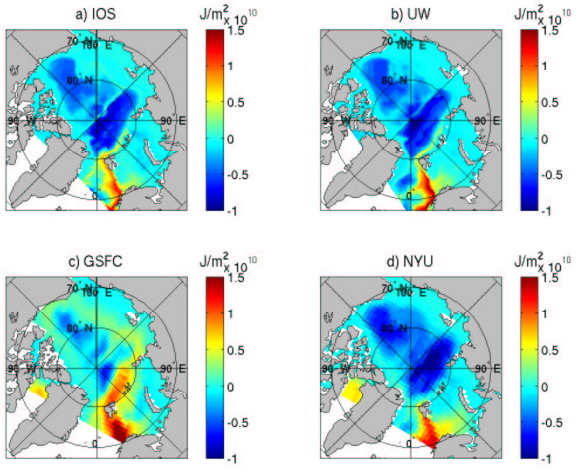

Figure 4: Annual average fields of internal heat energy for (a) IOS, (b) UW, (c) GSFC, and (d) NYU models. Note that the temperature data applied in the computation is relative to the 0°C.

Because of the close dependence on topography, the vertically integrated spatial distributions of IE presented in Figure 4 are calculated from temperatures relative to the 0°C. Then the contrast between the warm Atlantic and the cold Arctic water masses is better illustrated. The models have apparent differences how far into the Arctic Ocean the warm Atlantic water spreads. GSFC model seem to have the farthest inflow of the Atlantic water, while the warm water of NYU model seem to remain in the Barents Sea, which seem to be close to the average field of PHC in Figure 2a.

The seasonal variability of IE is biggest in the Greenland Sea and the Barents Sea. All models also reveal variability along the Canadian coast and in the archipelago. These are the regions of seasonal ice cover or totally ice–free and due to this the energy exchange with the atmosphere is more intensive. The results resemble the heat content estimates of Steiner et al. (2002, submitted manuscript). When compared with the PHC deviation in Figure 2b, the models seem to reveal less variability along the Barents-Arctic Shelf edge.

NYU model reveals high variability in the Beaufort Gyre, where for example IOS model has a variance of the same magnitude, but over a much more restricted region of seasonal ice near the coast of Alaska. The high variance of the NYU model has a much larger spatial scale and is linked to the changes in the model's circulation pattern and high velocities, which in turn seem to be connected to the high air–ocean momentum flux. The average sea-ice circulation pattern of the model is dominated by a clockwise gyre in the Beaufort Sea due to the applied climatological wind forcing. Modeled ocean currents follow closely this pattern with high mixed layer velocities of 10–20 cm/s. This indicates high stresses between the sea-ice and the mixed layer. This ice–ocean stress depends on difference between the sea-ice velocity and the velocity of the lower ocean layer, and on the drag coefficient at the interface. The air-ice drag coefficient of NYU model is 1.5×10^{-3} and ice-water drag coefficient 4.5×10^{-3}, which are, in fact, smaller than ones applied, for example, in IOS model. IOS model has drag coefficients 2.75×10^{-3} and 5.5×10^{-3} for the air–ice and ice–ocean interfaces, respectively. The high ice–ocean stress of NYU model can be explained by greater difference between the sea-ice velocity and the velocity of the ocean below.

4.2 *Kinetic energy*

The mutual coherence of KE between the models is significantly lower and the level of the relative variability much higher than with IE. The average KE values vary from 54 to 400 J m^{-2}, while the deviation is about half of the average level. The typical KE magnitude can be estimated of 100 J m^{-2}, but is sensitive to the changes in U because of the quadratic dependence of (1). The average KE of UW is significantly lower than the other models', while NYU model has the highest average KE.

As mentioned already in the section 4.1 the NYU model's high KE level is resulting from the strong air-ocean momentum flux. However, the deviations from average KE values are high and don't suggest significant bias of NYU KE level compared to the ones of GSFC and UW. This indicates the high average KE of NYU model is resulted from a local anomaly increasing correspondingly the deviation and to be mainly in ice covered regions, especially the Canadian basin. There might be a difference between an isopycnal model and a z-coordinate model when applying ice–ocean drag coefficients of close values. This follows because isopycnal NYU model treats mixed layer as a single numerical layer while z-coordinate model has several numerical levels inside the mixed layer. The reference ocean velocity of the ice-ocean stress is distinct for these two type of models. The uppermost ocean layer velocity of the z-coordinate model can be expected to be closer to the ice velocity than the one of the isopycnal model. Therefore with the same drag coefficient more stress is transferred to the ocean surface layer of the isopycnal model, because the ice–ocean velocity difference is higher. For example, IOS model has the uppermost level thickness of 2.5 m, while the mixed layer thickness of NYU model is more than 10 m.

The seasonal patterns (Figure 3c) deviate a lot, and NYU model has even an apparent inverse correspondence when compared with the other models. IOS, UW and GSFC models have relatively similar seasonal fluctuations, although the average values and deviations have differences of magnitude. These models have high KE levels in August – December.

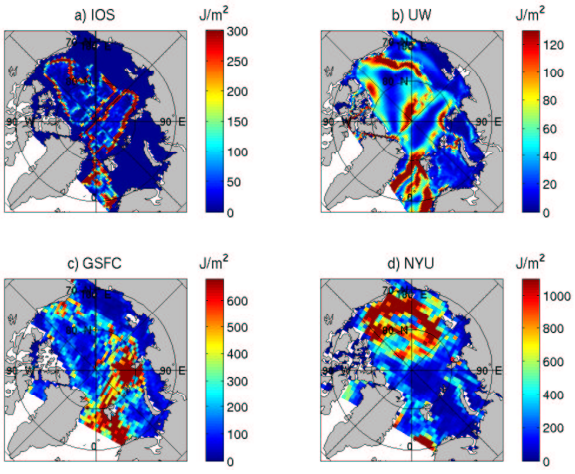

Figure 5: Annual average fields of kinetic energy for (a) IOS, (b) UW, (c) GSFC, and (d) NYU models.

Spatially the kinetic energy seem to be concentrated along the pathways of inflowing Atlantic water (see Figure 5), and in the Beaufort Gyre, especially with NYU model in Figure 5d. High energy levels in the Beaufort Sea are mostly responsible of the NYU model's high average KE. The increasing resolution seem to give a more distinctive pattern (Figure 5b) for KE, which is similar to the pattern of lower resolution IOS model (Figure 5a). IOS model utilizes

the Neptune parameterization (Nazarenko et al. (1998)), where the sub-grid scale eddies are interacting the bottom topography yielding a driving force of model resolved flows.

Shallow regions have small KE due to the smaller vertical integral. Central, deep parts of the Canadian and Eurasian basins have relatively small KE due to relatively low modeled velocities, whereas Barents–Siberian shelf edge and Beaufort Sea have higher velocities at all depths. This pattern reveals the Arctic Ocean circulation composed of the Transpolar Drift, the Beaufort Sea Gyre, the East Greenland Current and the Norwegian Coastal Current. NYU has high KE over Beaufort Sea Gyre and small, often almost non-existing Transpolar Drift. The KE variation is high at the same regions where the KE is high (Figure 5), but there are areas where the variance is small compared to the mean level of KE. These are located particularly in the Chukchi Sea (UW model), the Beaufort Sea (UW and IOS models) and the Canadian basin (NYU model).

4.3 *Potential energy and available potential energy*

PE is dominated by the topography of the basin. Accordingly, the modeled PE cycles follow relatively close to each other (Figure 3b). More interesting is APE, which interacts with KE. We estimate the magnitude of APE to be 10^5 J m^{-2}, assuming $\rho - \tilde{\rho} \simeq 1$ kg m^{-3}, and $\partial\widetilde{\rho_\phi}/\partial z \simeq -0.01$ kg m^{-4}. We calculate APE_O, which depends on the inverse of the vertical gradient of the potential density that tends to be large in the deep ocean and the anomaly from the horizontally averaged density, which tends to be large near the surface (5). These two terms, based on relatively small differentials, produce a combination, which is quite sensitive to uncertainties in the source terms. Therefore the significant differences due to the models and a random noise, due to, for example, numerical discretization, is difficult to distinguish. In the analysis we neglect the values of $\partial\widetilde{\rho_\phi}/\partial z < 5 \times 10^{-3}$ kg m^{-4}, which are considered to be below the numerical accuracy.

The annual average values of APE_O obtained from the models vary between 2 and 4×10^4 J m^{-2}, which are lower than the values presented by O94 and Oort et al. (1989). O94 obtained values of 4×10^5 J m^{-2} for the northern hemisphere based on the Levitus (1982) atlas for the ice-free ocean regions. The AOMIP models represent a relatively shallow Arctic basin and a mostly ice-covered regions, which decreases APE_O. In addition the reference density field $\tilde{\rho}$ is derived from the Arctic Ocean, while O94 applied a global mean value producing larger $\rho - \tilde{\rho}$.

The relative deviation of APE_O is quite large, having the same magnitude as the average values. These uncertainties can be seen from the seasonal cycle in Figure 3d, where the deviation between the models is apparent. However, there is a significant correlation of 0.96 between NYU and GSFC models, with the 95% confidence levels of $[0.86 \ldots 0.99]$. Those models also have evident seasonal cycles, which is apparent for PHC derived data. Temporal changes in APE_O are connected to $C(APE, KE)$ and also to the temporal changes in KE according to (2) and (6).

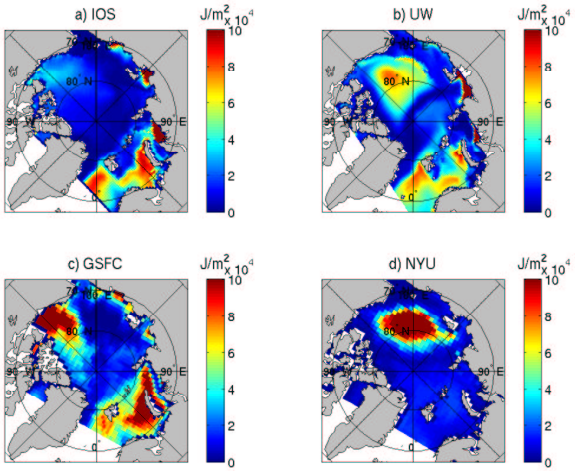

Figure 6: Annual average fields of available potential energy APE_O for (a) IOS, (b) UW, (c) GSFC, and (d) NYU models.

The average spatial distribution of the APE_O is presented in Figure 6 and in Figure 2c, where the two common regions of high APE_O are apparent, one in the Beaufort Gyre (NYU, UW, GSFC and PHC) and another in the Barents Sea (IOS, UW, GSFC and PHC). NYU model has high APE_O values in the Beaufort Sea due to the large light, relatively fresh water amount of the uppermost hundred meters producing large deviation of density from $\tilde{\rho}$. In the Barents Sea $(\rho - \tilde{\rho})^2$ is large because there the presence of the Atlantic water results in a large deviation from the average density profile of the Arctic Ocean.

IOS, UW, GSFC and PHC indicate higher APE_O levels near the mouths of the major Siberian rivers, which is not apparent in NYU model. The fresh river water inflow produces high APE_O with the same mechanism as is the case with high APE_O of NYU model in the Beaufort Sea. NYU model has no river discharge as a forcing, but its sea surface salinity is restored to PHC climatology. Although this restoring produces fresh water in front of the river mouths, most of the fresh water is located in the center of the anticyclonic gyre in the Canadian Basin. This fresh water mass dominates the spatial distribution of the NYU model's APE_O.

The seasonal variation of APE_O is smaller than the mean field magnitude, which is in accordance with O94 and PHC derived field in Figure 2d. The highest variability of the models is concentrated to the coastal regions indicating the variability of river discharge and sea-ice cover. In addition IOS, UW, GSFC and PHC have high variability in the Barents Sea, which is not apparent for NYU model.

4.4 *About the energy balance of the models*

The energy rate terms of equations (2) and (6) were calculated, but produced large deviations and small averages. O94 estimated annual average of $C(APE,KE)$ for the northern hemisphere to be -0.45$\times 10^{-3}$ W m^{-2}. Especially the values of IOS and UW models are close to this estimate. Their deviation σ, however, is large compared to the mean values, and the sign can change depending on the region from where the mean value is computed. GSFC model has one magnitude larger negative conversion rate and NYU model large positive conversion rate. Positive conversion rates seem to be connected to the strong vertical and low horizontal diffusion rates (O94).

Positive $C(APE,KE)$ takes place through sinking of relatively dense water and the rising of relatively light water (O94). Many processes at varying scales are involved with this convection, and are probably not resolved completely by ocean circulation models. The sign of $C(APE,KE)$ also depends on the chosen reference density profile. When the reference density represents the average density of the region, it results local $C(APE,KE)$ to vary around zero and the average $C(APE,KE)$ to be small. NYU model has a positive mean $C(APE,KE)$, which can be explained by the prevailing clockwise gyre in the Canadian Basin causing convergence of light water inside the gyre. In fact, the highest $C(APE,KE)$ values are concentrated over that region. Positive $C(APE,KE)$ is obtained from (7) when convergent velocity causes upward motion and a positive w along with a negative $(\rho - \tilde{\rho})$.

Horizontal velocity gradients may cause light water to sink or dense water to rise via the continuity equation. Here KE contributes to the APE and $C(APE,KE)$ is negative. This seem to be the mean state for the other models than NYU model. The highest negative $C(APE,KE)$ values seem to be obtained along the Barents-Arctic Siberian Shelf edge, when Atlantic water flows into the Arctic Ocean contributing to high APE values. GSFC model's negative $C(APE,KE)$ could be explained by its far-reaching Atlantic water inflow (see Figure 4).

O94 estimated the forcing rates $G(KE)$ and $G(APE)$ to be 4.2×10^{-3} W m^{-2} and 5×10^{-3} W m^{-2}, respectively, for the northern hemisphere. Their corresponding values for the dissipation rates $D(KE)$ and $D(APE)$ were 4×10^{-3} W m^{-2} and 5.4×10^{-3} W m^{-2}, respectively. One may expect conversion rates one magnitude smaller than the forcing and dissipation terms. The calculations of $D(APE)$ and $D(KE)$ based on the model fields produce unrealistic statistics and were excluded from the analysis. One reason for the sensitivity and large discrepancies are probably due to the inaccurate velocity, especially vertical, gradient fields. These relatively coarse fields do not present spatial scales of dissipation and thus do not produce correct results. Energy rate quantities like $D(KE)$, $D(APE)$ and $C(APE,KE)$, however, can be obtained directly from a model output with an energy analysis build into the model code (Ivchenko et al. (1997)).

5. CONCLUSIONS

We have analyzed the energetics of the four Arctic Ocean models focusing on the intercomparison of the model results. Major reasons for discrepancies between the models are probably the varying external forcing and boundary conditions applied. Partly due to this reason a new set of AOMIP model experiments are been constructed. The new set will produce results of the models where the forcing and boundary conditions are uniformly defined. The AOMIP forcing data is available and the model results will be distributed via AOMIP Live Access Server (LAS) at http://hamish.cims.nyu.edu/las.

Although the external factors affecting models are crucial, the energetics analysis reveals information of the model's internals as well. The discrete distributions of the energy components depend significantly on the grid definitions of the model. Further the statistics, which are calculated from these distributions are dependent on the grid definitions. This effect will remain even once the external forcing will be made the same. The more sophisticated the derived energy quantities are, the more sensitive they are to the grid density and numerical errors due to the discretization as well.

IE depends on the water temperature and density fields, which are relatively slowly varying and have small horizontal gradients. It is the most robust energy component of our analysis and all the models produce coherent IE fields. NYU model deviates most from the others with lower average IE. This model also has the shortest extent of the warm Atlantic water inflow into the Arctic Ocean.

The models have KE fields with high gradients producing large deviations from the average values. KE values were high along the major pathways (the Beaufort Gyre, the Transpolar Drift, the East Greenland Current and the Norwegian Coastal Current) guided by the basin's topography. The seasonal variability of the IOS and UW was low, but relatively similar. IOS model applies the Neptune parameterization producing a circulation pattern, which resembles the pattern of UW model. UW model has higher resolution, but doesn't utilize the Neptune parameterization.

The river discharge and seasonal ice cover result in variable APE_O fields at the coastal areas near the river mouths. NYU model has high APE_O in the Beaufort Gyre caused by the density anomaly produced by the model due to the too strong ice–ocean drag with high current speed in the mixed layer. According to a modeling experiment by Holland (1996), the Arctic Ocean circulation is weaker with smaller air–ocean stress, yet the basic pattern remains unchanged. The extensive Beaufort Gyre and weak Transpolar Drift of NYU model follows probably from the applied wind climatology, because preliminary results with the model show that the Transpolar Drift appear with daily wind forcing. The widespread Beaufort Gyre could partly prevent the existence of the Transpolar Drift. GSFC model also reveals high APE_O in the Beaufort Sea, but in the more coastal region.

UW model has high APE_O in the Beaufort Gyre, which is a persistent pattern with a low seasonal variability.

After the new set of AOMIP experiments have been completed with similar forcing, the analysis presented in this paper will be carried out for the new model data. By comparing results presented here with the new ones, one can qualitatively distinguish the effects of the external forcing on the energetics of Arctic Ocean models.

Acknowledgments Petteri Uotila thanks the International Arctic Research Center (IARC) and the Academy of Finland for their support of his research activities at NYU. David M. Holland is grateful to the NSF for support through grant OPP-0084286.

References

Häkkinen, S., 1999: A simulation of thermohaline effects of a great salinity anomaly. *J. Climate*, **12**, 1781-1795.

Holland, D. M., 2001: An impact of sub-grid-scale ice-ocean dynamics on sea ice cover. *J. Climate*, **14**, 1585-1601.

Holland, D. M., L. A. Mysak, and J. M. Oberhuber, 1996: Simulation of the mixed-layer circulation in the Arctic Ocean. *J. Geophys. Res.*, **101**, 1111-1128.

Holloway, G., and T. Sou, 2002: Has Arctic sea ice rapidly thinned ? *J. Climate*, **15**, 1691-1701.

Huang, R. X., 1998: Mixing and Available Potential Energy in a Boussinesq Ocean. *J. Phys. Oceanogr.*, **28**, pp. 669-678.

Ivchenko, V. O., A. M. Trequirer, S. E. Best, 1997: A Kinetic energy Budget and Internal Instabilities in the Fine Resolution Antarctic Model. *J. Phys. Oceanogr*, **27**, pp. 5-22.

Levitus, S., 1982: *Climatological Atlas of the World ocean*. NOAA Prof. Pap. 13, 17 microfiches, U. S. Government Printing Office, Washington, D. C., 163 pp.

Levitus, S. and T. Boyer, 1994: *NOAA Atlas NESDIS: World Ocean Atlas 1994*. US Dept. of Commerce, NOAA/NESDIS, Washington, DC.

Nazarenko, L., G. Holloway and N. Tausnev, 1998: Dynamics of transport of "Atlantic signature" in the Arctic Ocean. *J. Geophys. Res.*, **103**, pp. 31,003-31,015.

Oort, A. H., L. A. Anderson and J. P. Peixoto, 1994: Estimates of the energy cycle of the oceans. *J. Geophys. Res.*, **99**, C4, pp. 7665-7688.

Oort, A. H., S. C. Ascher, S. Levitus and J. P. Peixoto, 1989: New Estimates of the available potential energy in the World ocean, *J. Geophys. Res.*, **94**, C3, pp. 3187-3200.

Peixoto, J. P. and A. H. Oort, 1992: *Physics of Climate*. American Institute of Physics, New York, 520 pp.

Proshutinsky, A., M. Steele, J. Zhang, G. Holloway, N. Steiner, S. Häkkinen, D. Holland, R. Gerdes, C. Koeberle, M. Kärcher, M. Johnson, W. Maslowski, W. Walczowski, W. Hibler and J. Wang, 2001: Multinational Effort Studies Differences Among Arctic Ocean Models. *EOS*, **82**, 51, pp. 637-644.

Steele, M., W. Ernold, S. Häkkinen, D. Holland, G. Holloway, M. Kärcher, F. Kauker, W. Maslowski, N. Steiner and J. Zhang, 2001a: Adrift in the Beaufort Gyre: A Model Intercomparison. *Geophys. Res. Lett.*, **28**, pp. 2935-2938.

Steele, M., R. Morley, and W. Ermold, 2001b:, PHC: A global ocean hydrography with a high quality Arctic Ocean. *J. Climate*, **14**, 2079-2087.

Winters, K.B., P.N. Lombard, J.J. Riley and E.A. D'Asaro, 1995: Available potential energy and mixing in density-stratified fluids. *J. Fluid Mech.*, **289**, pp. 115-128.

Zhang, J., D. Rothrock, M. Steele, 2000: Recent changes in Arctic sea ice: The interplay between ice dynamics and thermodynamics. *J. Climate*, **13**, 3099-3114.